

## Study of the reverse saturation current and series resistance of p-p-n perovskite solar cells using the single and double-diode models

M.A. Cappelletti<sup>a,b,c,\*</sup>, G.A. Casas<sup>c,d</sup>, A.P. Cédola<sup>c,e</sup>, E.L. Peltzer y Blanca<sup>a,c</sup>, B. Marí Soucase<sup>f</sup>

<sup>a</sup> Comisión Nacional de Investigaciones Científicas (CONICET), Argentina

<sup>b</sup> Universidad Nacional Arturo Jauretche (UNAJ), Avenida Calchaquí 6200, Florencio Varela, 1888, Buenos Aires, , Argentina

<sup>c</sup> Grupo de Estudio de Materiales y Dispositivos Electrónicos (GEMyDE), Dpto. Electrotecnia, Facultad de Ingeniería, Universidad Nacional de La Plata, Calle 48 y 116, La Plata, 1900, Buenos Aires, Argentina

<sup>d</sup> Universidad Nacional de Quilmes, Roque Saenz Peña 352, Bernal, 1876, Buenos Aires, Argentina

<sup>e</sup> Comisión de Investigaciones Científicas, Provincia de Buenos Aires (CIC), Argentina

<sup>f</sup> Departament de Física Aplicada-ETSED, Universitat Politècnica de València, Camí de Vera s/n, València, 46022, Spain

### ARTICLE INFO

#### Keywords:

Perovskite solar cells  
Hole Transporting Material (HTM)  
One and two-diode models  
Genetic algorithm  
Parameters extraction

### ABSTRACT

The effects of the offset level and of the doping level in the perovskite layer upon both the reverse saturation current ( $J_0$ ) and the series resistance ( $R_s$ ) of p-p-n perovskite solar cells have been researched in this paper, using five different materials such as spiro-OMeTAD, Cu<sub>2</sub>O, CuSCN, NiO and CuI, as Hole Transporting Material (HTM). The analysis was carried out by means of the single and double-diode models of a solar cell and of genetic algorithms based on optimization technique, in order to extract the desired parameters. The minor degradation of  $J_0$  and  $R_s$  has been found for the condition offset equal to zero and for the highest doping level in p-type perovskite layer. Also, a comparison has been made of the behavior of two reverse saturation currents ( $J_{01}$  and  $J_{02}$ ). The power conversion efficiency (PCE) has shown to be more strongly dependent on  $J_{02}$  than on  $J_{01}$ . Results obtained in this work can be used to improve the manufacturing process of these devices.

### 1. Introduction

Energy is a strategic resource for the development of any country. The continuous increase in energy demand together with the associated environmental impact of fossil fuel combustion is strong incentives to promote the study and development of new technologies based on renewable energies such as photovoltaic (PV) and wind power generation systems. Solar energy is the most promising renewable energy source to generate electric power and to reduce the carbon dioxide (CO<sub>2</sub>) emissions to the atmosphere.

The study of materials and their microscopic properties together with the development of advanced device fabrication processes has opened the way to new research possibilities in photovoltaic technology in order to improve the performance of the PV cells.

In the last years, research on perovskite solar cells has attracted the interest of the scientific community due to its high power conversion efficiency (PCE) at low cost [1–6]. Experimental studies of the perovskite solar cells have reported a significant increase in PCE, from 3.8% in 2009 [7] to 22.7% recently [8], confirming the upward trend of this promising technology. Moreover, these

\* Corresponding author. Universidad Nacional Arturo Jauretche (UNAJ), Avenida Calchaquí 6200, Florencio Varela, 1888, Buenos Aires, Argentina.

E-mail address: [mcappelletti@unaj.edu.ar](mailto:mcappelletti@unaj.edu.ar) (M.A. Cappelletti).

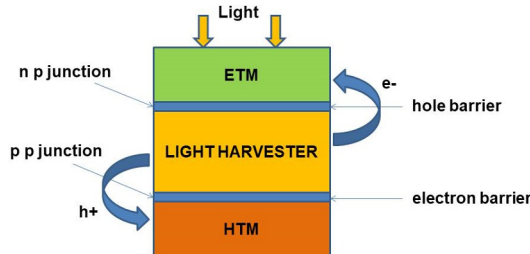


**Fig. 1.** The planar structure of a perovskite solar cell.

devices can be used to generate a solar-to-hydrogen conversion in water photolysis applications [9]. Therefore, further experimental and theoretical studies are required in order to have a better understanding of the behavior of perovskite solar cells and to optimize the design of the structure and the selection of materials.

A typical planar structure of perovskite solar cells composed of three regions: HTM/Perovskite/ETM is shown in Fig. 1, where HTM and ETM are the p-type hole-transporting material and the n-type electron-transporting material, respectively. The solar energy is absorbed by the p-type central material called perovskite layer, where after the charge carriers are photogenerated and extracted towards the electrodes, by transporting holes and electrons through the HTM and ETM layers, respectively.

A comparative theoretical study of perovskite solar cells of structure HTM/CH<sub>3</sub>NH<sub>3</sub>PbI<sub>3</sub>/TiO<sub>2</sub> has been recently developed by the authors through computer simulation using an organic compound (spiro OMeTAD) and four different inorganic materials (Cu<sub>2</sub>O, CuSCN, NiO and CuI) as HTM layer [10]. These inorganic compounds are promising candidates to replace the less stable and more expensive organic compound spiro-OMeTAD (2,2',7,7'-tetrakis (N,N-di-p-methoxyphenylamine)-9,9'-spirobifluorene). The five materials considered as HTM layer have different band gap energies ( $E_g$ ) and electron affinities ( $X_e$ ), which leads to different alignments between the Maximum of the Valence Band (MVB) of both the HTM and the perovskite layers, which is referred as the offset level ( $\text{Offset} = \text{MVB}_{\text{HTM}} - \text{MVB}_{\text{Perovskite}}$ ). The results obtained in Ref. [10] have shown a strong dependence of PCE with both the offset level and the doping level in p-type perovskite layer. Also, since Cu<sub>2</sub>O is the material with the lowest offset level (0.06 eV), the highest value of PCE has been obtained for the Cu<sub>2</sub>O/CH<sub>3</sub>NH<sub>3</sub>PbI<sub>3</sub>/TiO<sub>2</sub> solar cell.

For a better and more detailed understanding of the behavior of the perovskite solar cells, new studies on the same group of devices analyzed in Ref. [10] are presented here. Specifically, in this work, the effects of the offset level and of the doping level in the perovskite layer upon both the reverse saturation currents and the series resistance of these devices have been researched by means of the single and double-diode models of a solar cell and of a home-made numerical code based on genetic algorithms. The authors have previously used genetic algorithms based on optimization technique in order to extract the parameters of GaAs sub-cells for triple junction space solar cells [11].

The study of the reverse saturation currents is very useful to determine which conduction mechanism is predominant: the diffusion or the recombination process. It is possible to use the single or double-diode models for extraction of perovskite solar cell parameters since the planar-structured solar cells can in general be treated as a single p-n junction diode [12]. Different planar perovskite solar cells have been studied in Ref. [12] using the single-diode model.

## 2. Material and methods

### 2.1. Extraction of solar cells parameters

The current-voltage output characteristic ( $J-V$ ) of solar cells provides information about different parameters of interest of the devices, such as photocurrent, reverse saturation current, ideality factor, series resistance and shunt resistance. Having an accurate

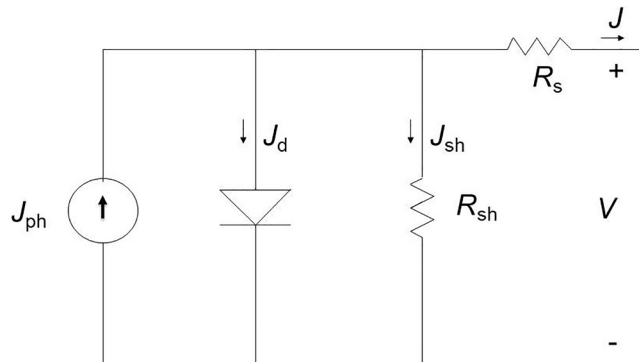


**Fig. 2.** Equivalent circuit model of a solar cell: (a) The one-diode model, and (b) The two-diode model.

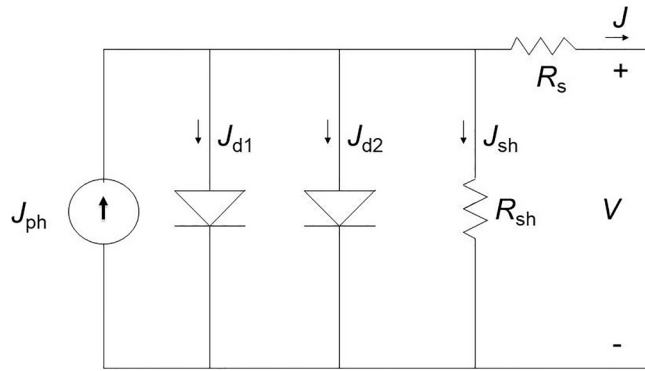


Fig. 2. (continued)

knowledge of these parameters is essential for evaluating the performance of the solar cells, for optimizing devices structure, for improving the fabrication process as well as in devices modelling and simulation [13,14]. These parameters can be accurately extracted from equations corresponding to the single or double diode models, which are the two main equivalent circuit models widely used to describe the nonlinear I–V behavior of a solar cell with or without illumination. These models are basically derived from the semiconductor equations that govern the physics of solar cells [15].

In the first case, one diode is connected in parallel to a light generated current source ( $J_{ph}$ ), such as is shown in Fig. 2(a), where  $J_d$  and  $J_{sh}$  are the current densities through the diode and the shunt resistance, respectively. The series resistance  $R_s$  represents the ohmic losses in the semiconductor bulk and in the metallic contacts, whereas the shunt resistance  $R_{sh}$  represents the current leakages across the p-n junction. Finally,  $J$  and  $V$  are the output current and the output voltage of the solar cell respectively, which are related through the following equation [16]:

$$J(V) = J_{ph} - J_d - J_{sh} = J_{ph} - J_0 \left\{ \exp \left[ \frac{q(V + JR_s)}{nkT} \right] - 1 \right\} - \frac{V + JR_s}{R_{sh}} \quad (1)$$

where  $J_0$  is the reverse saturation current of diode,  $n$  is the diode ideality factor,  $q$  is the electronic charge,  $k$  is the Boltzmann's constant and  $T$  is the temperature in kelvin.

On the other hand, Fig. 2(b) shows the double diode equivalent circuit model, where two diodes are connected in parallel to the current source and therefore a new current component with an exponential term is added to equation (1). This model allows to obtain a better understanding of the physical phenomena within the device, since it can be used to study the space charge recombination effect. The current  $J_{d1}$  represent the diffusion mechanism, including the recombination and drift occurring in the bulk material; and the current  $J_{d2}$  corresponds to the carrier recombination and generation in the space-charge region of the junction and to surface recombination [17]. The  $R_s$  and  $R_{sh}$  are similar to those corresponding to the one-diode model. In this case, the output current  $J$  and the output voltage  $V$  are related by Ref. [18]:

$$\begin{aligned} J(V) = & J_{ph} - J_{d1} - J_{d2} - J_{sh} = J_{ph} - J_{01} \left\{ \exp \left[ \frac{q(V + JR_s)}{n_1 kT} \right] - 1 \right\} \\ & - J_{02} \left\{ \exp \left[ \frac{q(V + JR_s)}{n_2 kT} \right] - 1 \right\} - \frac{V + JR_s}{R_{sh}} \end{aligned} \quad (2)$$

where  $J_{01}$  and  $J_{02}$  are the reverse saturation currents of diodes 1 and 2, respectively. Also,  $n_1$  and  $n_2$  are the diode ideality factors, respectively.

From equations (1) and (2), it can be seen that for modelling the I–V characteristics of a solar cell, it is necessary to extract five ( $J_{ph}$ ,  $J_0$ ,  $R_s$ ,  $R_{sh}$ ,  $n$ ) and seven ( $J_{ph}$ ,  $J_{01}$ ,  $J_{02}$ ,  $R_s$ ,  $R_{sh}$ ,  $n_1$ ,  $n_2$ ) parameters, respectively. These equations describe the performance of a solar cell under illumination or in dark conditions. However, they are transcendental equations that cannot be solved algebraically. Hence, the use of optimization methods to extract the unknown parameters are required.

Many parameters extraction techniques using equations (1) and (2) have been proposed in the literature, such as the Newton–Raphson Method (NRM) and the Levenberg–Marquardt Algorithm (LMA), which are both based on the gradient descent approach [19]. In recent years, heuristic methods such as genetic algorithms, have been used to improve the accuracy and computational efficiency for extraction of solar cell parameters as compared to conventional techniques, due to their known advantages related to the global minimum finding, easy of coding, etc. [11,20,21]. The genetic algorithms method, inspired by the biological evolution process, is based on the global search and optimization techniques [22]. This method does not determine a unique solution since there may be more than one combination of input parameters that yields the same output value. However, it is a powerful tool for obtaining approximate solutions to the exact solutions.

## 2.2. Simulation details

With the aim to understanding the behavior of different p-p-n perovskite solar cells, a numerical code based on genetic algorithms, fully developed by the authors in Python, has been used in order to extract the reverse saturation current, the series resistance

**Table 1**  
Characteristic parameters of the twelve solar cells under study.

Solar Cell	HTM	Offset (eV)	$N_A$ ( $\text{cm}^{-3}$ )
SC_1	Cu <sub>2</sub> O	0.06	$10^{17}$
SC_2	CuSCN	0.13	$10^{17}$
SC_3	NiO	0.17	$10^{17}$
SC_4	CuI	0.23	$10^{17}$
SC_5	spiro-OMeTAD	0.32	$10^{17}$
SC_6	Cu <sub>2</sub> O	0	$10^{17}$
SC_7	Cu <sub>2</sub> O	0.16	$10^{17}$
SC_8	Cu <sub>2</sub> O	0.26	$10^{17}$
SC_9	Cu <sub>2</sub> O	0.36	$10^{17}$
SC_10	Cu <sub>2</sub> O	0.06	$10^{18}$
SC_11	Cu <sub>2</sub> O	0.06	$10^{19}$
SC_12	Cu <sub>2</sub> O	0.06	$10^{20}$

and the ideality factor from equations (1) and (2). In particular, twelve devices of planar structure HTM/CH<sub>3</sub>NH<sub>3</sub>PbI<sub>3</sub>/TiO<sub>2</sub> have been analyzed, which are similar to those studied in Ref. [10], where HTM is one of the following materials: Cu<sub>2</sub>O, CuSCN, NiO, CuI and spiro-OMeTAD. Table 1 displays the complete set of the solar cells researched in this work, where the offset level is defined as  $\text{Offset} = MVB_{\text{HTM}} - MVB_{\text{Perovskite}}$ ; and  $N_A$  is the acceptor carrier concentration in the perovskite layer. It is considered that the solar radiation enter through the n-type transparent conducting oxide TiO<sub>2</sub>. The standard AM1.5G spectrum (1000 Wm<sup>-2</sup>; T = 300 K) has been used.

Table 2 summarizes the main physical parameters used for each layer in the one-dimensional code SCAPS-1D (Solar Cells Capacitance Simulator) [23] in order to obtain the I–V characteristic of the solar cells described in Table 1, where  $E_g$  is the band gap energy,  $X_e$  is the electron affinity,  $N_C$  and  $N_V$  are the effective density of states (DOS) in the conduction and the valence bands, respectively;  $\mu_n$  and  $\mu_p$  are the electron and hole mobilities, respectively;  $\epsilon$  is the relative permittivity; and  $N_A$  and  $N_D$  are the acceptor and donor carrier concentrations, respectively. These values are similar to those used by authors in Ref. [10].

The genetic algorithm based on optimization technique used in this work was implemented according to the following considerations:

- Binary representation is used as a solution encoding.

**Table 2**  
Main physical parameters used for each layer in the SCAPS-1D software.

	Cu <sub>2</sub> O	CuSCN	NiO	CuI	spiro-OMeTAD
HTM (400 nm)	$E_g$ (eV) $X_e$ (eV) $N_C$ ( $\text{cm}^{-3}$ ) $N_V$ ( $\text{cm}^{-3}$ ) $\mu_n$ ( $\text{cm}^2\text{V}^{-1}\text{s}^{-1}$ ) $\mu_p$ ( $\text{cm}^2\text{V}^{-1}\text{s}^{-1}$ ) $\epsilon$ $N_A$ ( $\text{cm}^{-3}$ ) $N_D$ ( $\text{cm}^{-3}$ )	2.17 3.2 $2.50 \times 10^{20}$ $2.50 \times 10^{20}$ 80 80 6.6 $3.00 \times 10^{18}$ 0	3.6 1.7 $2.50 \times 10^{20}$ $2.50 \times 10^{20}$ 25 25 5.1 $3.00 \times 10^{18}$ 0	3.8 1.46 $2.50 \times 10^{20}$ $2.50 \times 10^{20}$ 2.8 2.8 11.7 $3.00 \times 10^{18}$ 0	3.1 2.1 $2.50 \times 10^{20}$ $2.50 \times 10^{20}$ 44 44 6.5 $3.00 \times 10^{18}$ 0
Perovskite (400 nm)	$E_g$ (eV) $X_e$ (eV) $N_C$ ( $\text{cm}^{-3}$ ) $N_V$ ( $\text{cm}^{-3}$ ) $\mu_n$ ( $\text{cm}^2\text{V}^{-1}\text{s}^{-1}$ ) $\mu_p$ ( $\text{cm}^2\text{V}^{-1}\text{s}^{-1}$ ) $\epsilon$ $N_A$ ( $\text{cm}^{-3}$ ) $N_D$ ( $\text{cm}^{-3}$ )	1.5 3.93 $2.50 \times 10^{20}$ $2.50 \times 10^{20}$ 50 50 30 $1.00 \times 10^{17}$ 0			
TiO <sub>2</sub> (90 nm)	$E_g$ (eV) $X_e$ (eV) $N_C$ ( $\text{cm}^{-3}$ ) $N_V$ ( $\text{cm}^{-3}$ ) $\mu_n$ ( $\text{cm}^2\text{V}^{-1}\text{s}^{-1}$ ) $\mu_p$ ( $\text{cm}^2\text{V}^{-1}\text{s}^{-1}$ ) $\epsilon$ $N_A$ ( $\text{cm}^{-3}$ ) $N_D$ ( $\text{cm}^{-3}$ )	3.26 4.2 $1.00 \times 10^{21}$ $2.00 \times 10^{20}$ $1.00 \times 10^{-3}$ $1.00 \times 10^{-3}$ 100 $5.00 \times 10^{18}$ $5.00 \times 10^{19}$			

- The fitness function is based on equations (1) and (2), expressed as:

$$\begin{aligned} f(J_{\text{ph}}, J_0, R_s, R_{\text{sh}}, n) &= J_{\text{ph}} - J - J_{\text{d}} - J_{\text{sh}} \\ &= J_{\text{ph}} - J - J_0 \left\{ \exp \left[ \frac{q(V+JR_s)}{nkT} \right] - 1 \right\} - \frac{V+JR_s}{R_{\text{sh}}} \end{aligned} \quad (3)$$

and

$$\begin{aligned} f(J_{\text{ph}}, J_{01}, J_{02}, R_s, R_{\text{sh}}, n_1, n_2) &= J_{\text{ph}} - J - J_{\text{d}1} - J_{\text{d}2} - J_{\text{sh}} \\ &= J_{\text{ph}} - J - J_{01} \left\{ \exp \left[ \frac{q(V+JR_s)}{n_1 kT} \right] - 1 \right\} \\ &\quad - J_{02} \left\{ \exp \left[ \frac{q(V+JR_s)}{n_2 kT} \right] - 1 \right\} - \frac{V+JR_s}{R_{\text{sh}}} \end{aligned} \quad (4)$$

respectively.

- Random selection of the initial population.
- Initial population size: 500 individuals.
- Roulette wheel is used as method of selecting individuals for reproduction.
- The one-point crossover is employed with the crossover probability 0.7.
- Mutation probability 0.005.
- The genetic algorithm is executed 1000 generations.

The input data for the genetic algorithm are a set of  $N = 50$  values taken from each  $J$ - $V$  curve. The optimum solution is achieved when the fitness function is  $f(\dots) = 0$  for any  $J$ - $V$  pair. The Root Mean Square Error ( $RMSE$ ) is used in order to evaluate the performance of the technique based on genetic algorithms, which is calculated as:

$$RMSE = \sqrt{\frac{1}{N} \sum_{i=1}^N f_i(\dots)^2} \quad (5)$$

### 3. Results and discussion

#### 3.1. Analysis with the one-diode model of a solar cell

Five parameters, such as  $J_{\text{ph}}$ ,  $J_0$ ,  $R_s$ ,  $R_{\text{sh}}$  and  $n$ , can be extracted from the single diode model of a solar cell. It is often assumed that the light generated current density,  $J_{\text{ph}}$ , to be equal to the short-circuit current density  $J_{\text{sc}}$  [19]. Additionally, the effect of  $R_{\text{sh}}$  can be negligible. Thus, the solar cell parameter extraction problem reduces to the determination of three parameters:  $J_0$ ,  $R_s$  and  $n$ , from the  $J$ - $V$  characteristics. An efficient solar cell structure would possess low values in both parameters:  $J_0$  and  $R_s$ .

The results obtained of the extraction of  $J_0$  and  $R_s$  using genetic algorithms (GA) for the complete set of the solar cells studied in this work are summarized in the second and third column of Table 3, respectively. An optimum value of  $n$  equal to 1.44 has been extracted and fixed in all cases. The fourth column presents the  $RMSE$  values calculated with equation (5). Table 3 also presents the values of short-circuit current density  $J_{\text{sc}}$ , open circuit voltage  $V_{\text{oc}}$  and power conversion efficiency  $PCE$ , which were obtained from the SCAPS-1D software.

As can be observed in Table 3 the values of  $V_{\text{oc}}$  and  $PCE$  suffer significant variations with respect to both the offset level and the acceptor carrier concentration in the perovskite layer, whereas no changes were obtained in the values of  $J_{\text{sc}}$  for all devices considered here. Therefore, for the purpose of a better understanding of this behavior, an analysis of the data of  $J_0$  and  $R_s$  taken from

**Table 3**

Parameters extraction results of the solar cells described in Table 1 using the one-diode model.

Solar Cell	$J_0$ (Acm $^{-2}$ ) (GA)	$R_s$ ( $\Omega$ ) (GA)	$RMSE$ (Acm $^{-2}$ ) (GA)	$J_{\text{sc}}$ (mA cm $^{-2}$ ) (SCAPS-1D)	$V_{\text{oc}}$ (V) (SCAPS-1D)	$PCE$ (%) (SCAPS-1D)
SC_1	$4.64 \times 10^{-17}$	0.34	$1.93 \times 10^{-3}$	23.64	1.22	25.06
SC_2	$1.18 \times 10^{-16}$	0.46	$4.42 \times 10^{-4}$	23.65	1.21	24.86
SC_3	$2.31 \times 10^{-16}$	0.59	$1.28 \times 10^{-3}$	23.65	1.21	24.57
SC_4	$7.21 \times 10^{-16}$	0.81	$3.47 \times 10^{-3}$	23.65	1.19	23.78
SC_5	$4.46 \times 10^{-15}$	1.35	$4.49 \times 10^{-3}$	23.65	1.12	21.79
SC_6	$2.35 \times 10^{-17}$	0.31	$2.35 \times 10^{-3}$	23.64	1.23	25.10
SC_7	$1.85 \times 10^{-16}$	0.56	$2.51 \times 10^{-4}$	23.64	1.21	24.44
SC_8	$1.22 \times 10^{-15}$	0.97	$3.77 \times 10^{-3}$	23.65	1.17	23.09
SC_9	$2.01 \times 10^{-14}$	1.63	$1.03 \times 10^{-3}$	23.65	1.09	20.99
SC_10	$9.20 \times 10^{-18}$	0.22	$2.11 \times 10^{-3}$	23.64	1.23	25.62
SC_11	$4.42 \times 10^{-18}$	0.15	$1.32 \times 10^{-3}$	23.65	1.26	26.64
SC_12	$2.59 \times 10^{-18}$	0.12	$1.30 \times 10^{-3}$	23.67	1.30	27.44

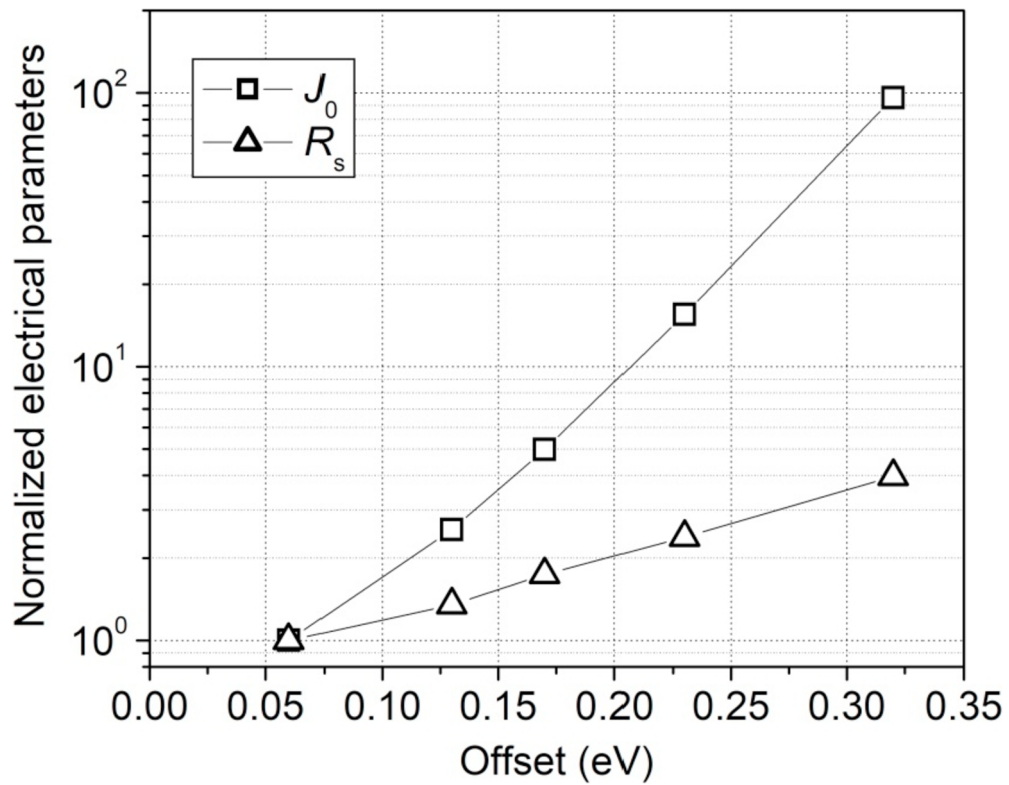


Fig. 3. Normalized electrical parameters as a function of the offset level for the five different HTM materials considered in this work.

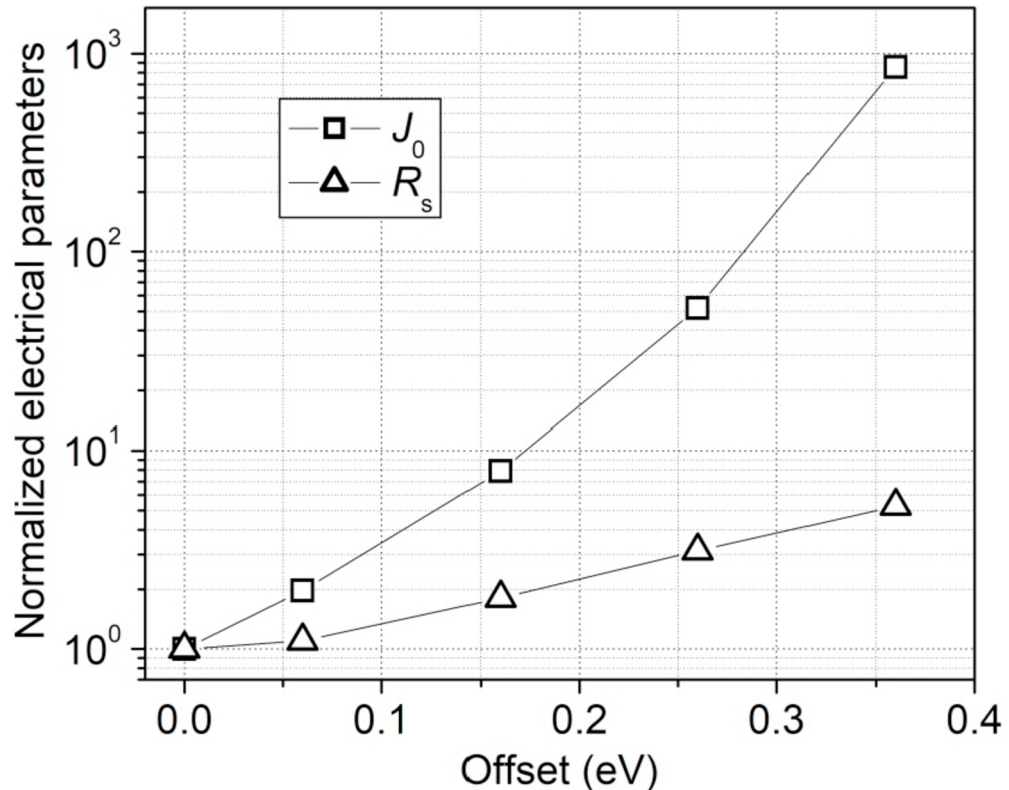
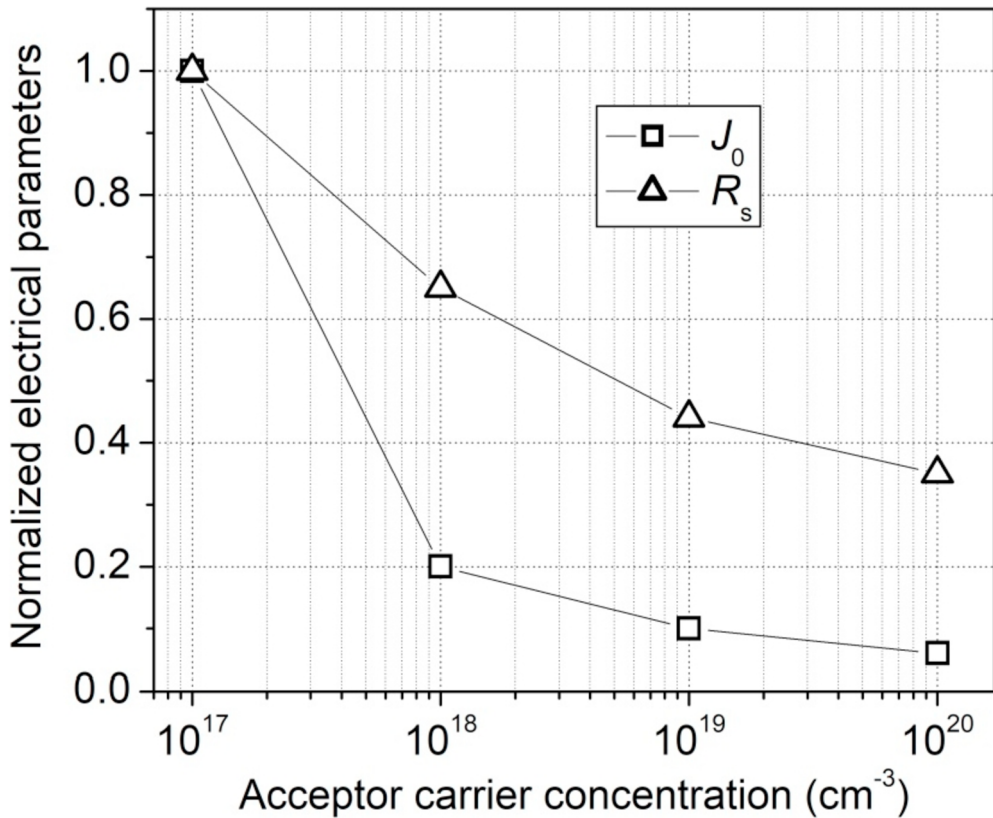


Fig. 4. Normalized electrical parameters as a function of the offset level for the  $\text{Cu}_2\text{O}/\text{Perovskite}/\text{TiO}_2$  solar cell.



**Fig. 5.** Normalized electrical parameters as a function of the acceptor carrier concentration in the perovskite layer for the  $\text{Cu}_2\text{O}/\text{Perovskite}/\text{TiO}_2$  solar cell.

**Table 4**

Parameters extraction results of the solar cells described in Table 1 using the two-diode model.

Solar Cell	$J_{01}$ ( $\text{Acm}^{-2}$ )	$J_{02}$ ( $\text{Acm}^{-2}$ )	RMSE ( $\text{Acm}^{-2}$ )	PCE (%)
SC_1	$6.81 \times 10^{-17}$	$1.91 \times 10^{-12}$	$1.41 \times 10^{-3}$	25.06
SC_2	$1.02 \times 10^{-16}$	$1.70 \times 10^{-11}$	$3.93 \times 10^{-4}$	24.86
SC_3	$1.43 \times 10^{-16}$	$3.52 \times 10^{-11}$	$2.24 \times 10^{-4}$	24.57
SC_4	$2.30 \times 10^{-16}$	$9.38 \times 10^{-11}$	$6.84 \times 10^{-4}$	23.78
SC_5	$8.14 \times 10^{-16}$	$3.50 \times 10^{-10}$	$3.84 \times 10^{-4}$	21.79
SC_6	$5.54 \times 10^{-17}$	$1.49 \times 10^{-13}$	$1.66 \times 10^{-3}$	25.10
SC_7	$1.28 \times 10^{-16}$	$2.88 \times 10^{-11}$	$1.21 \times 10^{-4}$	24.44
SC_8	$3.06 \times 10^{-16}$	$1.55 \times 10^{-10}$	$7.47 \times 10^{-4}$	23.09
SC_9	$2.04 \times 10^{-15}$	$4.98 \times 10^{-10}$	$4.73 \times 10^{-4}$	20.99
SC_10	$4.30 \times 10^{-17}$	$1.07 \times 10^{-14}$	$1.43 \times 10^{-3}$	25.62
SC_11	$3.04 \times 10^{-17}$	$1.04 \times 10^{-15}$	$3.98 \times 10^{-4}$	26.64
SC_12	$1.44 \times 10^{-17}$	$2.68 \times 10^{-16}$	$1.93 \times 10^{-4}$	27.44

Table 3 are shown in Fig. 3, Fig. 4 and Fig. 5. The lines through the data points are only intended to guide the eye.

Fig. 3 shows the variation of  $J_0$  and  $R_s$  parameters with respect to the offset level of the five different materials considered for the HTM layer (SC\_1, SC\_2, SC\_3, SC\_4 and SC\_5). The values presented are normalized to those corresponding to the offset level equal to 0.06 eV (i.e.  $\text{Cu}_2\text{O}$  as HTM layer), which are  $4.64 \times 10^{-17} \text{ Acm}^{-2}$  and  $0.34 \Omega$ , for  $J_0$  and  $R_s$ , respectively. This figure shows that  $J_0$  and  $R_s$  reach the lowest values for the  $\text{Cu}_2\text{O}/\text{CH}_3\text{NH}_3\text{PbI}_3/\text{TiO}_2$  heterojunction as compared to the corresponding parameters of the devices based on the other four hole-transport materials. It can also be seen an abrupt increase in  $J_0$  (close to 2 orders of magnitude) and a gradual increase of  $R_s$  (close to 4 times) when the offset level is increased. These significant increases in  $J_0$  and  $R_s$  could explain the reduction of the PCE, from 25.06% to 21.79% for  $\text{Cu}_2\text{O}$  and spiro-OMeTAD, respectively.

Since the  $\text{Cu}_2\text{O}$  is the material with the lowest real offset (0.06 eV), Figs. 4 and 5 show the results obtained of the extraction of electrical parameters on the  $\text{Cu}_2\text{O}/\text{CH}_3\text{NH}_3\text{PbI}_3/\text{TiO}_2$  solar cells. Specifically, Fig. 4 shows the normalized data ( $J_0$  and  $R_s$ ) as a function of the offset level (SC\_1, SC\_6, SC\_7, SC\_8 and SC\_9). The offset level was artificially modified by changing the electron affinity of  $\text{Cu}_2\text{O}$ . In this case, the values presented are normalized to those corresponding to the offset level equal to zero, which are

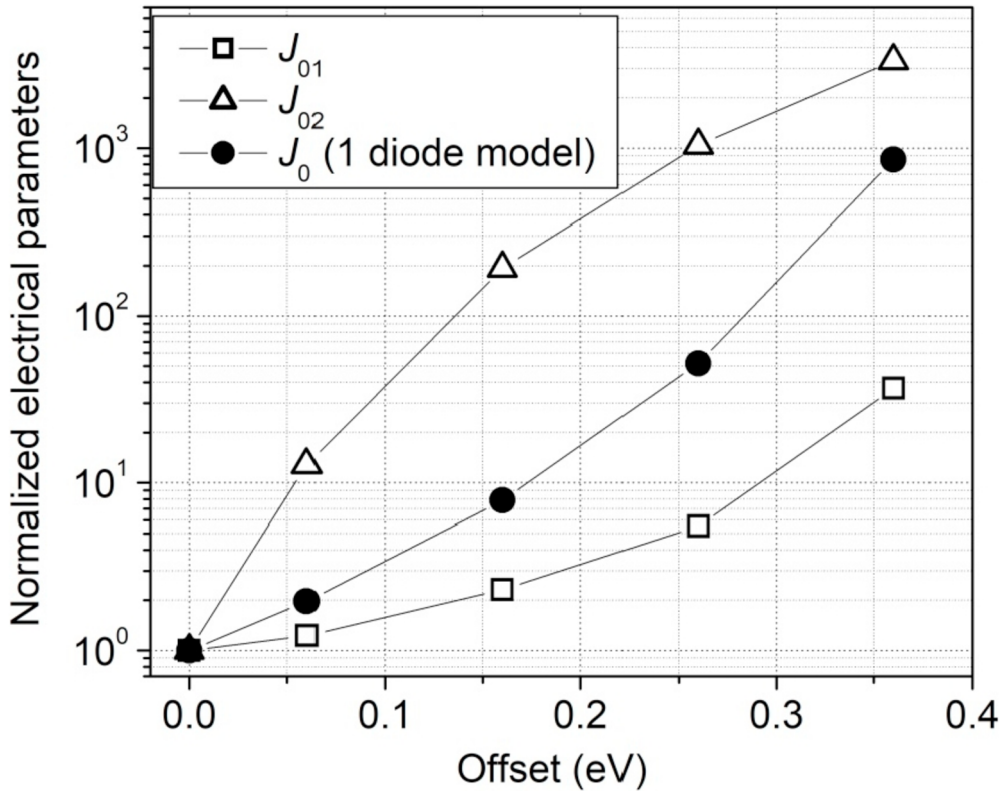


Fig. 6. Normalized electrical parameters as a function of the offset level for the Cu<sub>2</sub>O/Perovskite/TiO<sub>2</sub> solar cell.

$2.35 \times 10^{-17}$  Acm<sup>-2</sup> and  $0.31 \Omega$ , for  $J_0$  and  $R_s$ , respectively. The data set presented in Fig. 4 show a similar behavior to that described in Fig. 3. It can also be observed that the best condition to achieve the lesser degradation in  $J_0$  and  $R_s$  is obtained for when the offset level is equal to zero. Under this condition, no differences in the value of PCE were found using CuSCN, CuI and NiO as HTM layer, whereas for spiro-OMeTAD the value of PCE is reduced due to its very low value of hole mobility [10].

Finally, effects of the acceptor carrier concentration in the perovskite layer upon the  $J_0$  and  $R_s$  values are shown in Fig. 5 for the condition offset equal to 0.06 eV (SC\_1, SC\_10, SC\_11 and SC\_12). These values are presented as normalized with respect to those corresponding to the  $N_A$  equal to  $10^{17}$  cm<sup>-3</sup>, which are  $4.64 \times 10^{-17}$  Acm<sup>-2</sup> and  $0.34 \Omega$ , for  $J_0$  and  $R_s$ , respectively. It is possible to observe in this figure that when  $N_A$  is increased from  $10^{17}$  to  $10^{20}$  cm<sup>-3</sup>, then  $J_0$  and  $R_s$  decrease about 95% and 65%, respectively. Therefore, the decreasing of  $J_0$  and  $R_s$  could be the main reason for the increase of PCE from 25.06% to 27.44%.

### 3.2. Analysis with the two-diode model of a solar cell

The addition of a second diode to the previous model, makes it possible to study in more detail the space charge recombination effect. The second diode in the double-diode model contributes two additional parameters: the reverse saturation current  $J_{02}$  and the ideality factor  $n_2$ . Therefore, from this model seven parameters can be extracted,  $J_{ph}$ ,  $J_{01}$ ,  $J_{02}$ ,  $R_s$ ,  $R_{sh}$ ,  $n_1$  and  $n_2$ . In a similar way to the analysis carried out previously with the single-diode model, it was assumed that  $J_{ph} = J_{sc}$  and the effect of  $R_{sh}$  was considered negligible. Also, the  $R_s$  parameter was taken with the values presented in Table 3. Thus, in this case, from the J-V curves, the solar cell parameter extraction problem reduces to determination of four parameters:  $J_{01}$ ,  $J_{02}$ ,  $n_1$  and  $n_2$ .

Table 4 contains the results obtained using genetic algorithms of the extraction of  $J_{01}$  and  $J_{02}$  for the twelve solar cells studied in this work. The optimum values of  $n_1$  equal to 1.44 and of  $n_2$  equal to 2.50 have also been extracted and fixed in all cases. Ideality factors higher than 2 have also been obtained for different perovskite solar cells in Ref. [12]. The fourth column presents the RMSE values calculated with equation (5). Finally, for convenience, in Table 4 the values of PCE are also shown.

The values obtained for  $J_{01}$  and  $J_{02}$  in Table 4 are consistent with literature data since  $J_{02}$  is generally 3 to 7 orders of magnitude larger than  $J_{01}$  [18]. An analysis of the data of  $J_{01}$  and  $J_{02}$  taken from Table 4 are shown in Fig. 6 and Fig. 7.

Fig. 6 shows data of  $J_{01}$  and  $J_{02}$  as a function of the offset level on the Cu<sub>2</sub>O/CH<sub>3</sub>NH<sub>3</sub>PbI<sub>3</sub>/TiO<sub>2</sub> solar cells (SC\_1, SC\_6, SC\_7, SC\_8 and SC\_9). These values are normalized to those corresponding to the offset level equal to zero (SC\_6), which are  $5.54 \times 10^{-17}$  Acm<sup>-2</sup> and  $1.49 \times 10^{-13}$  Acm<sup>-2</sup>, for  $J_{01}$  and  $J_{02}$ , respectively. As a comparison, it has also been added in Fig. 6 the data of  $J_0$  shown previously in Fig. 4. It can be seen in Fig. 6 a much greater increase in  $J_{02}$  (close to 3300 times) than in  $J_{01}$  (close to 37 times), when the offset level is increased from 0 to 0.36 eV. Therefore, the decrease in PCE, from 25.10% to 20.99% is a major consequence of the

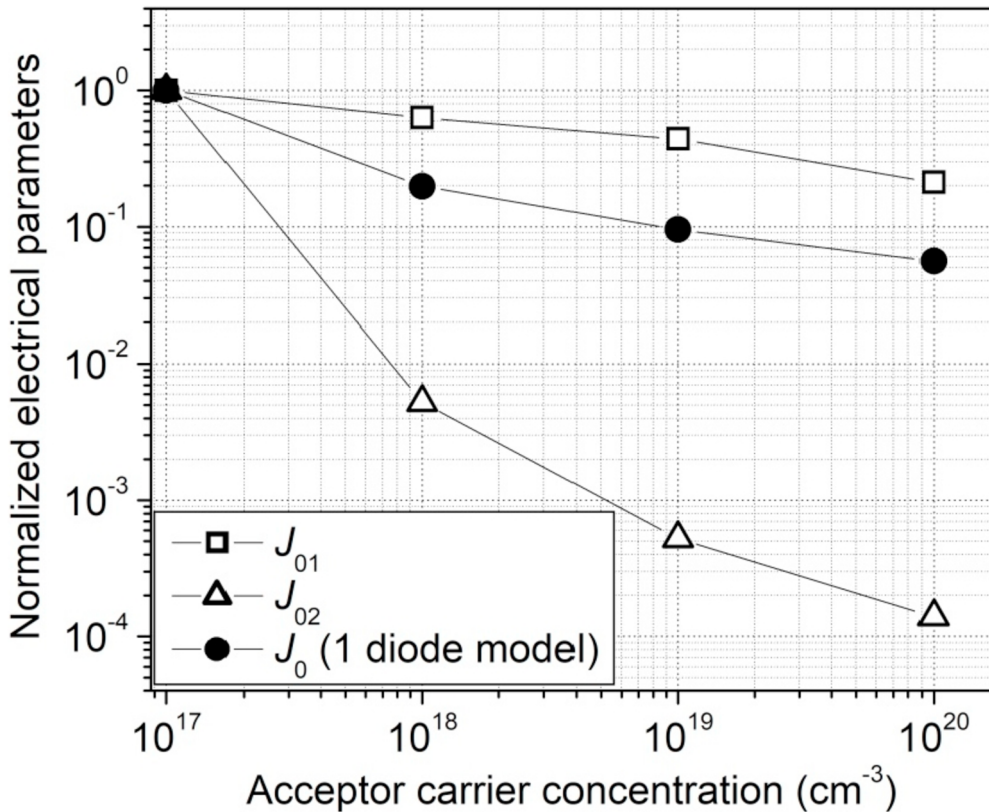


**Fig. 7.** Normalized electrical parameters as a function of the acceptor carrier concentration in the perovskite layer for the Cu<sub>2</sub>O/Perovskite/TiO<sub>2</sub> solar cell.

strong increase in the carrier recombination in the space-charge region of the junction.

Fig. 7 shows the normalized data for  $J_{01}$  and  $J_{02}$ , calculated by varying the acceptor carrier concentration in the perovskite layer (SC\_1, SC\_10, SC\_11 and SC\_12). The values presented are normalized to those corresponding to the  $N_A$  equal to  $10^{17} \text{ cm}^{-3}$ , which are  $J_{01} = 6.81 \times 10^{-17} \text{ Acm}^{-2}$  and  $J_{02} = 1.91 \times 10^{-12} \text{ Acm}^{-2}$ . Again, as a comparison, it has also been added in Fig. 7 the data of  $J_0$  shown previously in Fig. 5. In this case, it can be observed that when  $N_A$  is increased from  $10^{17}$  to  $10^{20} \text{ cm}^{-3}$ , then  $J_{02}$  decreases more strongly (close to 4 orders of magnitude) than  $J_{01}$  (about 80%), which tend to improve the solar cell performance.

In order to better understand the physical mechanisms of conduction present within the devices, we have plotted in Fig. 8 the variation of the current components through the two diodes,  $J_{d1}$  and  $J_{d2}$ , calculated as:

$$J_{d1,d2} = J_{01,02} \left\{ \exp \left[ \frac{q(V + JR_s)}{n_{1,2}kT} \right] - 1 \right\} \quad (6)$$

as a function of the voltage, for the two extreme cases: devices with the minimum and the maximum PCE values (SC\_9 and SC\_12, respectively).

Fig. 8 shows that for the SC\_9 device ( $PCE = 20.99\%$ ), the dominant effect from 0 V to  $V_{oc}$  is the minority carrier recombination in the space-charge region. On the contrary, for the SC\_12 device ( $PCE = 27.44\%$ ), two different behaviors occur within the device. At voltages below 0.25 V, the effect of  $J_{d2}$  is more significant than  $J_{d1}$ , whereas the current flow controlled by minority carrier diffusion outside the space-charge region is the dominant effect at voltages from 0.25 V to  $V_{oc}$ . For all solar cells considered in this work, the values of the slopes are  $\frac{q}{n_1 kT}$  and  $\frac{q}{n_2 kT}$  for  $J_{d1}$  and  $J_{d2}$ , respectively. Besides, it has been found that as the value of PCE increases from 20.99% to 27.44%, the value of voltage for which both mechanisms have the same effect ( $J_{d1} = J_{d2}$ ) decreases from 1.09 V to 0.25 V.

#### 4. Conclusion

The results obtained in this work have allowed us to study in detail the physical mechanisms of conduction present within the perovskite solar cells and are useful to contribute to the design, optimization and manufacturing process of such devices. This paper continues the research started in a recent work of the authors. In the study performed here, the behavior of the reverse saturation current and the series resistance of perovskite solar cells of structure HTM/CH<sub>3</sub>NH<sub>3</sub>PbI<sub>3</sub>/TiO<sub>2</sub> with five different Hole Transporting Material (HTM), such as spiro-OMeTAD, Cu<sub>2</sub>O, CuSCN, NiO and CuI, has been discussed. These parameters have been extracted using genetic algorithms based on optimization technique and the single and double-diode models of a solar cell. It has been observed that

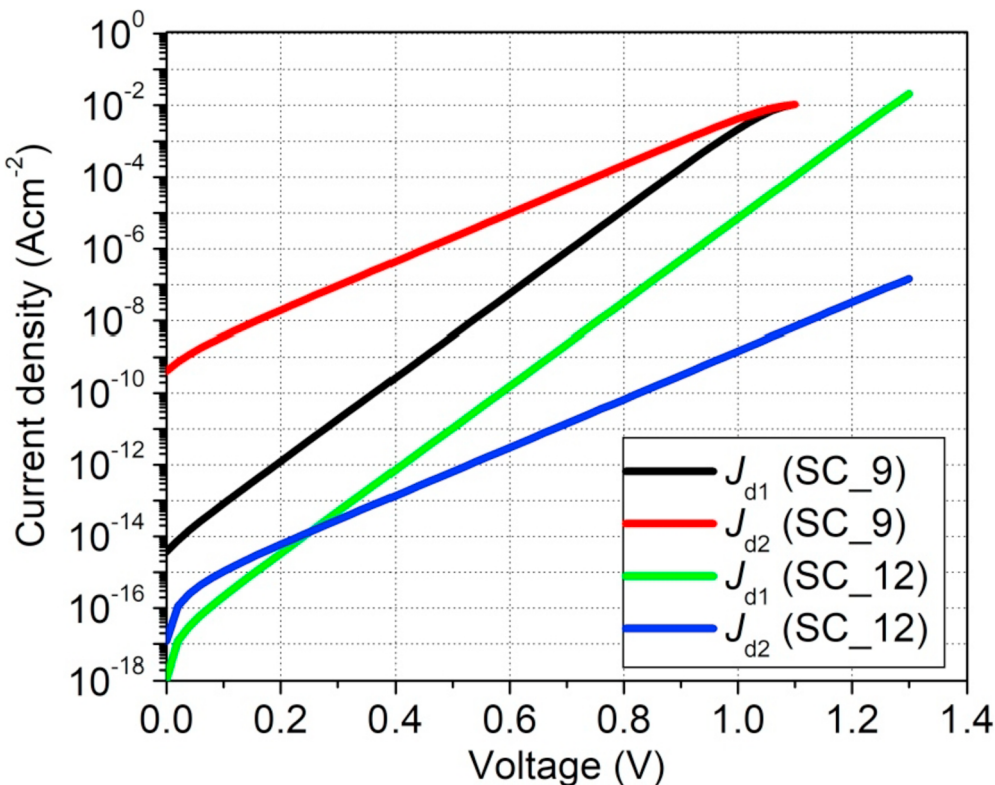


**Fig. 8.** Current density components-Voltage curves for two  $\text{Cu}_2\text{O}/\text{Perovskite}/\text{TiO}_2$  solar cells, with the minimum and maximum values of PCE.

these parameters are strongly dependent on both the alignment between the Maximum of the Valence Band (MVB) of the HTM and perovskite layers (offset level), and the doping level in p-type perovskite layer. Specifically, it has been obtained that the increase in the offset level from 0 to 0.36 eV, produces an abrupt increase in  $J_0$  (close to 3 orders of magnitude) and a gradual increase of  $R_s$  (close to 5 times), which could explain the reduction of the PCE from 25.10% to 20.99%. In opposition,  $J_0$  and  $R_s$  decrease about 95% and 65%, respectively in the case that the acceptor carrier concentration in the perovskite layer has gone increasing from  $10^{17}$  to  $10^{20} \text{ cm}^{-3}$ , which could be the main reason for the increase of PCE from 25.06% to 27.44%. Besides, a comparison has been made of the behavior of two reverse saturation currents ( $J_{01}$  and  $J_{02}$ ). It has been found that the offset level and of the doping level in the perovskite layer affect more strongly to  $J_{02}$  than  $J_{01}$ . Finally, it has also been found that when the carrier recombination and generation mechanisms in the space-charge region of the junction predominates over the carrier diffusion mechanism, including the recombination and drift occurring in the bulk material, the devices are less efficient. Therefore, the use of HTM materials with lower offset levels and p-type perovskites with higher doping levels would be good alternatives for the organic compound spiro-OMeTAD in order to reduce the cost and increase the performance of the devices.

## Funding

This work was partially supported by the National Council Research (CONICET), Argentina, by the Universidad Nacional Arturo Jauretche, Argentina, by the Universidad Nacional de Quilmes, Argentina, by the Universidad Nacional de La Plata, Argentina and by the Ministerio de Economía y Competitividad (Grant ENE2016-77798-C4-2-R), Spain.

## References

- [1] M. Javad Taghavi, et al., Modeling of optical losses in perovskite solar cells, *Superlattice. Microst.* 97 (2016) 424–428.
- [2] F. Liu et al., Numerical simulation: toward the design of high-efficiency planar perovskite solar cells, *Appl. Phys. Lett.* 104 (2014) 253508 (4pp).
- [3] A. Baktash, et al., Improve efficiency of perovskite solar cells by using Magnesium doped ZnO and TiO<sub>2</sub> compact layers, *Superlattice. Microst.* 93 (2016) 128–137.
- [4] K. Adhikari, et al., Comparative study on MAPbI<sub>3</sub> based solar cells using different electron transporting materials, *Phys. Status Solidi C* (2015) 1–5.
- [5] M. Green, et al., The emergence of perovskite solar cells, *Nat. Photon.* 8 (2014) 506–514.
- [6] C. Zuo, et al., Advances in perovskite solar cells, *Adv. Sci.* 3 (2016) 1500324(16pp).
- [7] A. Kojima, et al., Organometal halide perovskites as visible-light sensitizers for photovoltaic cells, *J. Am. Chem. Soc.* 131 (2009) 6050–6051.
- [8] National Renewable Energy Laboratory (NREL), Efficiency chart, (April, 2018) <https://www.nrel.gov/pv/assets/images/efficiency-chart.png>.
- [9] J. Luo, et al., Water photolysis at 12.3% efficiency via perovskite photovoltaics and Earth-abundant catalysts, *Science* 345 (2014) 1593–1596.
- [10] G. Casas, et al., Analysis of the power conversion efficiency of perovskite solar cells with different materials as Hole-Transport Layer by numerical simulations,

- Superlattice. Microst. 107 (2017) 136–143.
- [11] M. Cappelletti, et al., Study of the electrical parameters degradation of GaAs sub-cells for triple junction space solar cells by computer simulation, Semicond. Sci. Technol. 31 (2016) 115020.
  - [12] S. Chatterjee, A. Pal, Introducing Cu<sub>2</sub>O thin films as a Hole-Transport Layer in efficient planar perovskite solar cell structures, J. Phys. Chem. C 120 (2016) 1428–1437.
  - [13] R. Gottschalg, et al., The influence of the measurement environment on the accuracy of the extraction of physical parameters of solar cells, Meas. Sci. Technol. 10 (1999) 796–804.
  - [14] S. Yadir, et al., A new technique for extracting physical parameters of a solar cell model from the double exponential model (DECM), Opt. Mater. 36 (2014) 18–21.
  - [15] S. Sze, K. Ng, Physics of Semiconductor Devices, third ed., John Wiley & Sons, New Jersey, 2007.
  - [16] D. Chan, et al., A comparative study of extraction methods for solar cell model parameters, Solid State Electron. 29 (1986) 329–337.
  - [17] J.P. Charles, et al., Consistency of the double exponential model with physical mechanisms of conduction for a solar cell under illumination, J. Phys. Appl. Phys. 18 (1985) 2261–2268.
  - [18] M. Wolf, et al., Investigation of the double exponential in the current-voltage characteristics of silicon solar cells, IEEE Trans. Electron. Dev. 24 (1977) 419–428.
  - [19] J. Appelbaum, A. Peled, Parameters extraction of solar cells – a comparative examination of three methods, Sol. Energy Mater. Sol. Cells 122 (2014) 164–173.
  - [20] A. Zagrouba, et al., Identification of PV solar cells and modules parameters using the genetic algorithms: application to maximum power extraction, Sol. Energy 84 (2010) 860–866.
  - [21] J. Jervase, et al., Solar cell parameter extraction using genetic algorithms, Meas. Sci. Technol. 12 (2001) 1922–1925.
  - [22] M. Mitchell, An Introduction to Genetic Algorithms, Editorial MIT Press, 1999.
  - [23] M. Burgelman, et al., Modelling polycrystalline semiconductor solar cells, Thin Solid Films 361 (2000) 527–532.